Dynamic Behavior Analysis of a Rotating Smooth and Discontinuous Oscillator with Irrational Nonlinearity

Ning Han[1] & Mingjuan Liu[2]

[1] Key Lab. of Machine Learning and Computational Intelligence, College of Mathematics and Information Science, Hebei University, Baoding, China

[2] Medical College, Hebei University, Baoding, China

Correspondence: Ning Han, Main Building Office 511, Wusi East Road No.180, College of Mathematics and Information Science, Hebei University, Baoding, 071002, China. E-mail: han_ning@outlook.com

Abstract

This paper focuses on a novel rotating mechanical model which provides a cylindrical example of transition from smooth to discontinuous dynamics. The remarkable feature of the proposed system is a cylindrical dynamical system with strongly irrational nonlinearity exhibiting both smooth and discontinuous characteristics due to the geometry configuration. By using nonlinear dynamical technique, the unperturbed dynamics of the proposed system are studied including the irrational restoring force, stability of equilibria, Hamiltonian function and phase portraits. Note that a pair of double heteroclinic-like orbits connecting two non-standard saddle points are proposed in discontinuous case. For the perturbed system, we introduce a cylindrical approximate system for which the analytical solutions can be obtained successfully to reflect the nature of the original system without barrier of the irrationalities. Melnikov method is employed to detect the chaotic thresholds for the double heteroclinic orbits under the perturbation of viscous damping and external harmonic forcing in smooth regime. Finally, numerical simulations show the efficiency of the proposed method and demonstrate the predicated periodic solution and chaotic attractors. It is found that a good degree of correlation is demonstrated in the bifurcation diagram, the phase portraits of periodic solution, the chaotic attractor' structures and the Lyapunov characteristics between the original system and approximate system.

Keywords: SD oscillator, cylindrical dynamical system, irrational nonlinearity, Melnikov method, chaos

1. Introduction

It is well known that the simple pendulum is a typically cylindrical dynamical system, which is among the most widely investigated motions in physics and many nonlinear phenomena in the real world. In modern time, many kinds of pendulum-like systems or systems containing trigonometric function term have gained wide attention due to the cylindrical dynamic behavior, which greatly enrich the research content of cylindrical dynamical system. Briefly, Koch et al. investigated the boundaries of sub-harmonic and homoclinic bifurcations in a parametrically forced pendulum on the basis of Melnikov method and averaging method (Koch et al., 1984). Kwek et al. studied the sub-harmonic bifurcations and chaotic dynamics in a pendulum-like system (Kwek et al., 1996), which shows the cylindrical phase portraits coexisting with two types of homoclinic orbits and different types of chaos including pendulum type, duffing type and combined type. Yabuno et al. proved the bifurcation in an inverted pendulum with the high frequency excitation by using analytical and experimental investigations (Yabuno et al., 2004). Xu et al. discussed two typical responses of oscillations and rotations in a parametric pendulum by applying perturbation method (Xu et al.,2007).

Recently, a rotating pendulum linked by an oblique spring with fixed end has been proposed and investigated in (Cao et al., 2011). This system is a cylindrical dynamical system with irrational characters whose free motion is similar to the simple pendulum coupled with SD oscillator (Cao et al., 2006; Tian et al., 2010) of the homoclinic

orbits of the first and second type. The authors introduce a cylindrical approximate system for which the analytical solutions can be obtained successfully to reflect the nature of the rotating pendulum system without barrier of the irrationalities (Han et al., 2013). Then the chaotic boundary of discontinuous case with a pair of heteroclinic-like orbits (Han et al., 2015) are obtained by using semi-analytical method. The bifurcation of cylindrical dynamical system with double well can be investigated in (Han et al., 2016) by means of Melnikov method and numerical simulation. The dynamic response of a parametrically excited pendulum with irrational nonlinearity is examined, which exhibits bi-stable state and discontinuous characteristics due to the geometry configuration (Han et al., 2017).

This paper presents a novel rotating mechanical model, which is a typically cylindrical dynamical system with irrational nonlinearity exhibiting both smooth and discontinuous dynamics due to the geometrical configuration. The motivation of this paper is to detect the chaotic dynamics of the proposed cylindrical dynamical system by means of a cylindrical approximate system which efficiently reflects the nonlinear dynamics of the original system. This approach enables us to investigate the nonlinear dynamic behaviors theoretically for both the unperturbed and perturbed systems without using Taylor expansion. The proposed cylindrical dynamical system bears significant similarities to the original system of phase portraits with the double heteroclinic orbits which successfully avoids the barrier of the associated irrational nonlinearity.

2. Equation of Motion

In this section, a novel rotating mechanical model is illustrated, which comprises a lump mass linked by a pair of inclined elastic springs which are capable of resisting both tension and compression. Consider the rotating mechanical model moving on the horizontal plane as shown in Figure 1, subjected a viscous damping $CL\dot{x}$ and an external harmonic excitation of the amplitude F_0 and frequency ω in the direction of motion, for which the differential equation has the form

$$mL\ddot{x} + CL\dot{x} + k\alpha \cos x \left(\frac{l}{\sqrt{L^2 + \alpha^2 - 2L\alpha \sin x}} - \frac{l}{\sqrt{L^2 + \alpha^2 + 2L\alpha \sin x}} \right) = F_0 \cos \omega t \quad (1)$$

where the dot denotes derivative with respect to t, m is the lump mass, L is the length of mass-less rod, k and l are the stiffness and relax length of the spring, α is the half distance between the rigid supports, always assumed $\alpha \geq L$ respectively.
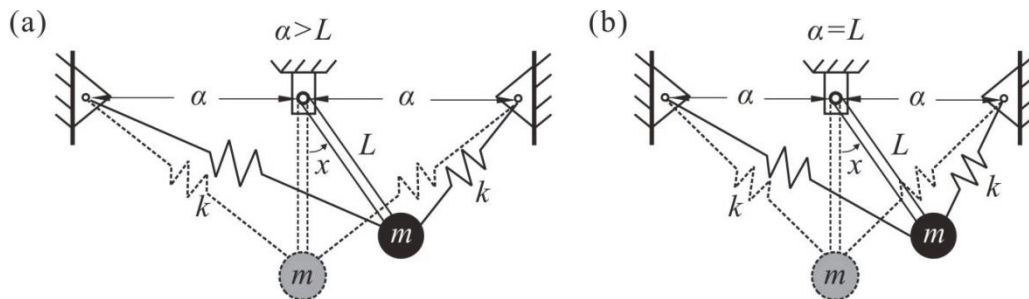

Figure 1. The model of rotating smooth and discontinuous oscillator, (a) smooth case for $\alpha > L$, (b) discontinuous case for $\alpha = L$.

It is worth pointing out that the dynamical system (1) can be smooth or discontinuous depending on the value of the smoothness parameter α. Note that system (1) is smooth for $\alpha > L$ as shown in Figure 1(a), while it is discontinuous for $\alpha = L$ as shown in Figure 1(b). It is worth reiterating here that the discontinuous dynamics is obtained by changing the parameter α to L smoothly, which is the limit case as $\alpha \to L$ from the mathematical point of view. Without loss of generality, nonlinear dynamical system (1) can be rewritten in the following form

$$\ddot{x} + \xi \dot{x} + \omega_0^2 \cos x \left(\frac{1}{\sqrt{1 + \lambda^2 - 2\lambda \sin x}} - \frac{1}{\sqrt{1 + \lambda^2 + 2\lambda \sin x}} \right) = f_0 \cos \omega t \quad (2)$$

where

$$\xi = \frac{C}{m}, \quad \omega_0 = \sqrt{\frac{kl}{mL}}, \quad \lambda = \frac{L}{\alpha}, \quad f_0 = \frac{F_0}{mL}.$$

It is worth noticing here that the transition occurs on system (2) from smooth case to discontinuous case when the smoothness parameter λ is increased to 1. More precisely, smooth dynamics appears when $\lambda < 1$, while the discontinuous behaviors occurs at $\lambda = 1$. From the view of physical meaning, parameter ω_0 is regarded as the natural frequency of system (1), λ mainly reflects the geometry structure of the mechanical model.

3. Unperturbed Dynamics

In this section, the unperturbed dynamics of the proposed system including the irrational restoring force, the stability of equilibria, the potential energy, the Hamiltonian function and phase portraits are discussed by using nonlinear dynamical technique (Guckenheimer et al., 2007) in both smooth and discontinuous case, respectively.
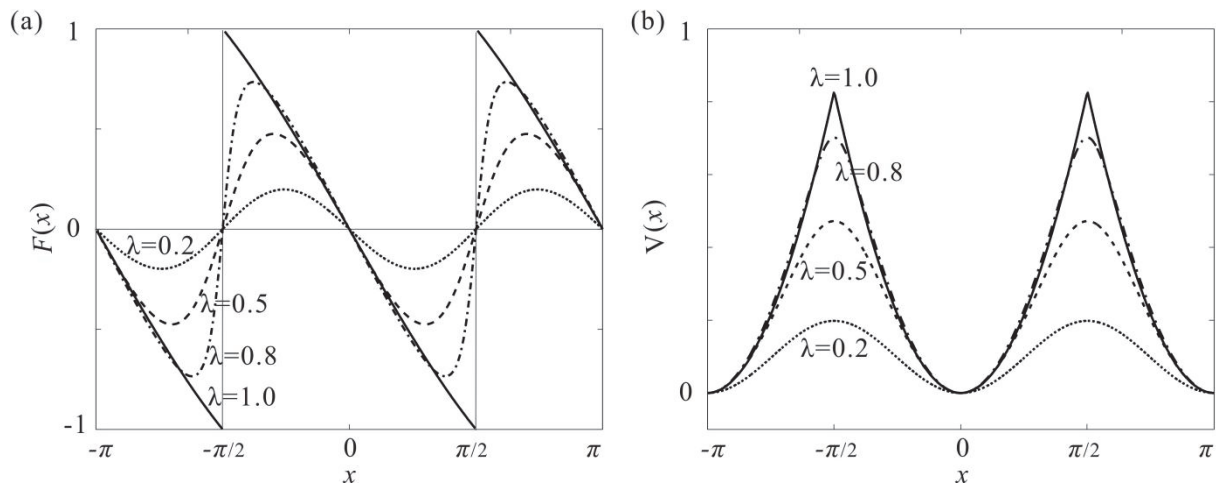

Figure 2. When $\omega_0 = 1$, (a) the nonlinear restoring forces of smooth case for $\lambda = 0.2, \ 0.5, \ 0.8$ and discontinuous case for $\lambda = 1.0$; (b) the corresponding potential energy of smooth case for $\lambda = 0.2, \ 0.5, \ 0.8$ and discontinuous case for $\lambda = 1.0$

When $\xi = 0$ and $f_0 = 0$, system (2) can be written as a two dimensional one

$$\dot{x} = y, \quad \dot{y} = -\omega_0^2 \cos x \left(\frac{1}{\sqrt{1 + \lambda^2 - 2\lambda \sin x}} - \frac{1}{\sqrt{1 + \lambda^2 + 2\lambda \sin x}} \right) \tag{3}$$

Letting $\dot{y} = F(x)$, the irrational restoring force of unperturbed system (3)

$$F(x) = -\omega_0^2 \cos x \left(\frac{1}{\sqrt{1 + \lambda^2 - 2\lambda \sin x}} - \frac{1}{\sqrt{1 + \lambda^2 + 2\lambda \sin x}} \right) \tag{4}$$

are plotted for smooth case $\lambda \in (0, \ 1)$ in Figure 2(a) for different values of parameter λ taking fixed $\omega_0 = 1$, marked by dotted line, dashed line, dash-dot line for $\lambda = 0.2, \ 0.5$ and 0.8, respectively. Especially when $\lambda = 1$, the nonlinear restoring force of discontinuous case can be written as

$$F_d(x) = -\omega_0^2 \left[\sin\left(\frac{\pi}{4} + \frac{x}{2} \right) \mathrm{sgn}\left(\cos\left(\frac{\pi}{4} + \frac{x}{2} \right) \right) - \cos\left(\frac{\pi}{4} + \frac{x}{2} \right) \mathrm{sgn}\left(\sin\left(\frac{\pi}{4} + \frac{x}{2} \right) \right) \right] \tag{5}$$

where

$$\text{sgn}\left(\cos\left(\frac{\pi}{4}+\frac{x}{2}\right)\right)=\begin{cases} 1, & x\in\left[-\pi,\dfrac{\pi}{2}\right), \\ 0, & x=\dfrac{\pi}{2}, \\ -1, & x\in\left(\dfrac{\pi}{2},\pi\right], \end{cases} \qquad \text{sgn}\left(\sin\left(\frac{\pi}{4}+\frac{x}{2}\right)\right)=\begin{cases} 1, & x\in\left(-\dfrac{\pi}{2},\pi\right], \\ 0, & x=-\dfrac{\pi}{2}, \\ -1, & x\in\left[-\pi,-\dfrac{\pi}{2}\right), \end{cases} \tag{6}$$

only consider over a period $x\in[-\pi,\pi]$. It is worth pointing out that the nonlinear restoring force $F_d(x)$ is discontinuous at $x=-\pi/2$ and $x=\pi/2$, satisfying

$$F_d\left(\frac{\pi^+}{2}\right)=\lim_{x\to\frac{\pi^+}{2}}F_d(x)=\omega_0^2, \ \ F_d\left(\frac{\pi^-}{2}\right)=\lim_{x\to\frac{\pi^-}{2}}F_d(x)=-\omega_0^2, \ \ F_d\left(\frac{\pi}{2}\right)=0,$$

$$F_d\left(-\frac{\pi^+}{2}\right)=\lim_{x\to-\frac{\pi^+}{2}}F_d(x)=\omega_0^2, \ \ F_d\left(-\frac{\pi^-}{2}\right)=\lim_{x\to-\frac{\pi^-}{2}}F_d(x)=-\omega_0^2, \ \ F_d\left(-\frac{\pi}{2}\right)=0,$$

Meanwhile, Figure 2(a) shows the nonlinear restoring force of discontinuous case taking fixed $\omega_0=1$ and $\lambda=1$, marked by solid line. Even the stiffness of the spring is linear and the resistance force supplied to the system (1) is strongly irrational nonlinearity due to geometry configuration.

The corresponding potential energy of smooth ($\lambda<1$) and discontinuous ($\lambda=1$) case

$$V(x)=-\frac{\omega_0^2}{\lambda}\left(\sqrt{1+\lambda^2-2\lambda\sin x}+\sqrt{1+\lambda^2+2\lambda\sin x}-2\sqrt{1+\lambda^2}\right) \tag{7}$$

are shown in Figure 2(b), respectively. Meanwhile, Figure 2(b) displays the standard and nonstandard double well dynamics denoted by dotted line, dashed line, dot-dash line and solid line, respectively. It is worth noticing here that the potential energy $V(0)$ is regarded as zero. Defining $F(x)=0$, the equilibria of system (3) can be written as

$$(x_1,y_1)=(0,0),\ (x_{2,3},y_{2,3})=(\pm\pi,0),\ (x_{4,5},y_{4,5})=\left(\pm\frac{\pi}{2},0\right)$$

The Jacobian matrix of the unperturbed system (3) at equilibria $(x_1,y_1)=(0,0)$ and $(x_{2,3},y_{2,3})=(\pm\pi,0)$ can be derived as

$$J_{(0,0),(\pm\pi,0)}=\begin{bmatrix} 0 & 1 \\ -2\omega_0^2\lambda\left(1+\lambda^2\right)^{-1.5} & 0 \end{bmatrix}$$

of which the eigenvalues are $\lambda_{1,2}=\pm\sqrt{2\omega_0^2\lambda\ (1+\lambda^2)^{-1.5}}\,i$. It is clear that the equilibria $(0,0)$ and $(\pm\pi,0)$ are stable center points for any parameter values. Similarly, the Jacobian matrix of system (3) at equilibria $(x_{4,5},y_{4,5})=(\pm\pi/2,0)$ can be obtained as

$$J_{(\pm\pi/2,0)}=\begin{bmatrix} 0 & 1 \\ \dfrac{2\omega_0^2\lambda}{1-\lambda^2} & 0 \end{bmatrix}$$

whose eigenvalues are $\lambda_{1,2}=\pm\sqrt{2\omega_0^2\lambda/(1-\lambda^2)}$, thus the equilibria $(\pm\pi/2,0)$ are saddle points for $\lambda<1$.

Particularly, it is found that the eigenvalues of system (3) do not exist when $\lambda=1$, the equilibria $(\pm\pi/2,0)$ are

saddle-like points (Cao et al., 2006). The Hamiltonian function of system (3) is given by

$$H(x,y) = \frac{y^2}{2} - \frac{\omega_0^2}{\lambda}\left(\sqrt{1+\lambda^2 - 2\lambda\sin x} + \sqrt{1+\lambda^2 + 2\lambda\sin x} - 2\sqrt{1+\lambda^2}\right) \tag{8}$$

By means of the Hamiltonian function (8), the trajectories of unperturbed system (3) can be classified and analyzed for different values of $H(x,y)=h$, the energy level, the detail seen in Figure 3(a) and (b). Smooth dynamics for $\lambda < 1$ is depicted in Figure 3(a), demonstrating a pair of double heteroclinic orbits, marked by *het*, connecting the points $(-\pi/2,0)$ and $(\pi/2,0)$, denoted by solid point. It is worth reiterating here that the smooth dynamics Figure 3(a) becomes discontinuous dynamics Figure 3(b) by increasing the smoothness parameter λ to 1. Similarly, the discontinuous dynamics for $\lambda = 1$ is plotted in Figure 3(b), demonstrating a pair of double heteroclinic-like orbits, marked by *Dhet*, connecting the points $(-\pi/2,0)$ and $(\pi/2,0)$, which exhibits non-smooth dynamics at $x = \pm\pi/2$. It is worth pointing out that the black solid points represent the standard equilibrium and the cycle mean the non-standard equilibrium, which is named as ``saddle-like'' points (Cao et al., 2006). Particularly, the phase trajectories marked by the dotted line and the dashed line correspond to the oscillations and rotations, respectively.
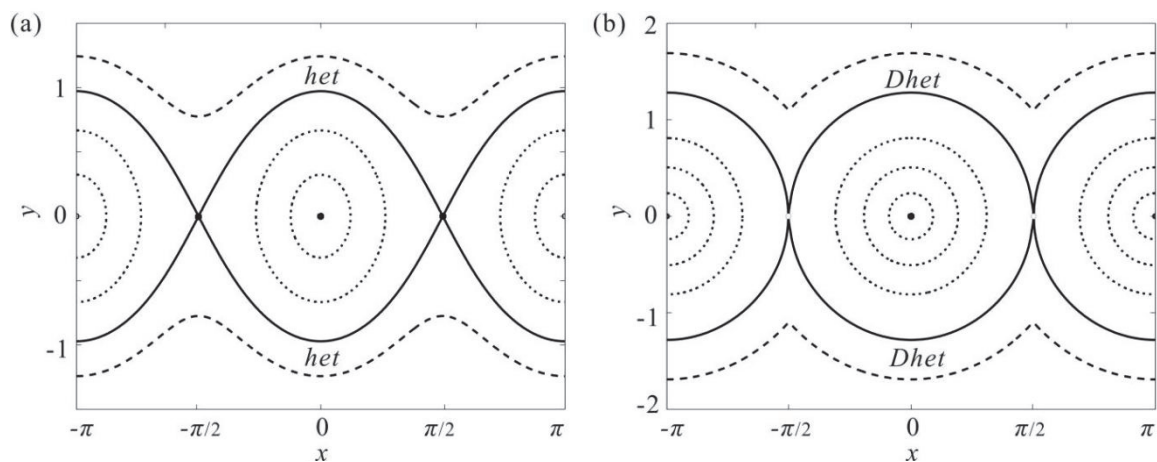

Figure 3. Phase portraits of unperturbed system for $\omega_0 = 1$: (a) smooth case for $\lambda = 0.5$, (b) discontinuous case for $\lambda = 1.0$. (the dotted and dashed curves represent oscillations and rotations respectively)
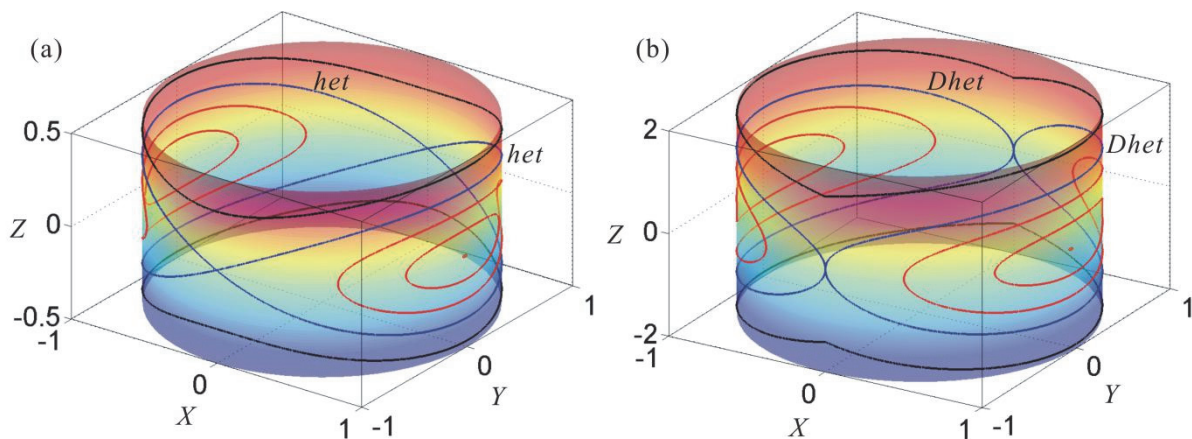

Figure 4. Cylindrical phase portraits for smooth and discontinuous case, (a) double well coexisting with two pairs of heteroclinic orbits (*het* colored in blue) for $\omega_0 = 1, \lambda = 0.5$; (b) double well coexisting with two pair of heteroclinic-like orbit (*Dhet* colored in blue) for $\omega_0 = 1, \lambda = 1$. (Online version in colour.)

Note that the state of the nonlinear dynamical system is unchanged by the addition of 2π to *x*, it is an advantage topologically to introduce a cylindrical phase space. The cylindrical dynamical equation can be derived by letting $X = \cos x, Y = \sin x, Z = \dot{x}$ and written as follow

$$\begin{cases} \dot{X} = -YZ \\ \dot{Y} = XZ \\ \dot{Z} = -\omega_0^2 X \left(\dfrac{1}{\sqrt{1+\lambda^2 - 2\lambda Y}} - \dfrac{1}{\sqrt{1+\lambda^2 + 2\lambda Y}} \right) \\ 1 = X^2 + Y^2 \end{cases} \tag{9}$$

of which the Hamiltonian can be written as follow

$$\begin{cases} H(X,Y,Z) = \dfrac{Z^2}{2} - \dfrac{\omega_0^2}{\lambda} \left(\sqrt{1+\lambda^2 - 2\lambda Y} + \sqrt{1+\lambda^2 + 2\lambda Y} - 2\sqrt{1+\lambda^2} \right) \\ X^2 + Y^2 = 1 \end{cases} \tag{10}$$

Based upon the Hamiltonian function (10), two typically cylindrical phase portraits are plotted for different values of $H(X, Y, Z) = h$, the energy level, the detail seen in Figure 4. Double well coexisting with a pair of double heteroclinic orbits (denoted by *het*) connecting two standard saddle equilibria is displayed for $\lambda = 0.5$ in Figure 4(a). Specially, Figure 4(b) shows double well coexisting with a pair of double heteroclinic-like orbits (denoted by *Dhet*) connecting two non-standard saddle equilibria for $\lambda = 1$. It is worth pointing out that the double heteroclinic orbits divided the cylindrical phase portraits into two parts, which means two types of movement. One is stand for the oscillating orbits colored in red and the other is the rotating orbits marked by black solid line.

4. Perturbed Dynamics

In this section, the perturbed dynamics for smooth system are investigated by using Melnikov method and numerical simulations. Specially, we introduce a simple cylindrical dynamical system with dynamic behavior approximately equivalent to the original system for parameter λ taking small value which successfully avoids the barrier of the associated irrational nonlinearity.

4.1 A Cylindrical Approximate System of Smooth Region for $\lambda \ll 1$

Defining $\omega_0 = 1$, the perturbed system (2) can be re-written as follow

$$\ddot{x} + \xi \dot{x} + \cos x \left(\frac{1}{\sqrt{1+\lambda^2 - 2\lambda \sin x}} - \frac{1}{\sqrt{1+\lambda^2 + 2\lambda \sin x}} \right) = f_0 \cos \omega t \tag{11}$$

Based upon the equilibria and the change of nonlinear restoring force in Figure 2(a), we define a cylindrical approximate system to reflect the dynamic behavior of system (11) for $\lambda \ll 1$, which successfully avoids the barrier of the associated irrational nonlinearity. When $\omega_0 = 1$ and $\lambda \ll 1$, the cylindrical approximate system can be regard as

$$\ddot{x} + \xi \dot{x} + A \sin 2x = f_0 \cos \omega t \tag{12}$$

where

$$A = \left| F\left(\frac{\pi}{4} \right) \right| = \frac{1}{\sqrt{2}} \left(\frac{1}{\sqrt{1+\lambda^2 - \sqrt{2}\lambda}} - \frac{1}{\sqrt{1+\lambda^2 + \sqrt{2}\lambda}} \right)$$

It is clear that the equilibria of the unperturbed approximate system (12) can be derived as $(-\pi/2, 0)$, $(0,0)$ and $(\pi/2, 0)$, which is similar to the original system (11). For $\omega_0 = 1$, the nonlinear restoring forces of the original system (11) and approximate system (12) are given by

$$\begin{cases} F(x) = -\cos x\left(\dfrac{1}{\sqrt{1+\lambda^2-2\lambda\sin x}} - \dfrac{1}{\sqrt{1+\lambda^2+2\lambda\sin x}}\right) \\[4mm] \overline{F(x)} = -\dfrac{1}{\sqrt{2}}\left(\dfrac{1}{\sqrt{1+\lambda^2-\sqrt{2}\lambda}} - \dfrac{1}{\sqrt{1+\lambda^2+\sqrt{2}\lambda}}\right)\sin 2x \end{cases} \tag{13}$$

Figure 5(a) shows the comparisons of nonlinear restoring forces between the original system (11) colored in red and approximate system (12) denoted by black dotted lines for $\omega_0 = 1$ and $\lambda = 0.01,\ 0.02,\ 0.03,\ 0.04$. It is worth pointing out that the maximum absolute error of nonlinear restoring forces $\left|F(x) - \overline{F(x)}\right|$ between the original system and approximate system is small than $7\times10^{-7}, 6\times10^{-6}, 2\times10^{-5}, 5\times10^{-5}, 7\times10^{-4}$ for $\omega_0 = 1$ and $\lambda = 0.01,\ 0.02,\ 0.03,\ 0.04,\ 0.1$, respectively. Then, the Hamiltonian function corresponding to the heteroclinic orbits of the original system (11) and approximate system (12) are given by

$$\begin{cases} \dfrac{y^2}{2} = \dfrac{1}{\lambda}\left(\sqrt{1+\lambda^2-2\lambda\sin x} + \sqrt{1+\lambda^2+2\lambda\sin x} - 2\lambda\right) \\[4mm] \dfrac{y^2}{2} = \dfrac{1}{\sqrt{2}}\left(\dfrac{1}{\sqrt{1+\lambda^2-\sqrt{2}\lambda}} - \dfrac{1}{\sqrt{1+\lambda^2+\sqrt{2}\lambda}}\right)\cos^2 x \end{cases} \tag{14}$$
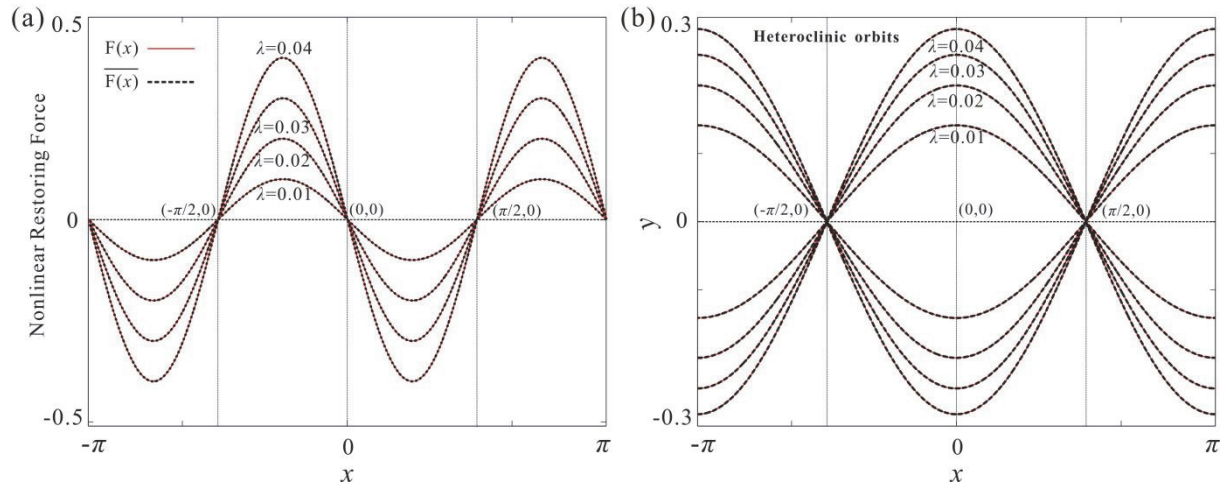

Figure 5. Graphs of the restoring forces and double heteroclinic orbits for the original (red solid line) and the approximate (black dashed line) systems when $\omega_0 = 1$: (a) nonlinear restoring forces for $\lambda = 0.01,\ 0.02,\ 0.03,\ 0.04$ and the corresponding double heteroclinic orbits (b), respectively. (Online version in colour.)

The comparisons of the double heteroclinic orbits between the original system colored in red and the approximate system denoted by black dashed lines are displayed for $\omega_0 = 1$ and $\lambda = 0.01,\ 0.02,\ 0.03,\ 0.04$ respectively, the detail seen in Figure 5(b). By comparison, it is found that the proximity of the nonlinear restoring forces and double heteroclinic orbits are very high, which means that the approximate system can successfully reflect the dynamic behavior of the original system. So the analytic solutions for the double heteroclinic orbits of the approximate system denoted by *het* connecting $(-\pi/2, 0)$ and $(\pi/2, 0)$ can be derived as

$$\left(x_\pm^{het}(t), y_\pm^{het}(t)\right) = \left(\pm\tan^{-1}\left(\sinh\left(\sqrt{2A}\,t\right)\right), \pm\sqrt{2A}\,\mathrm{sech}\left(\sqrt{2A}\,t\right)\right),\ \left(x_\pm^{het}(0), y_\pm^{het}(0)\right) = \left(0, \pm\sqrt{2A}\right)$$

4.2 Chaotic Thresholds of Smooth Case for $\lambda \ll 1$

The Melnikov function is proportional to the first variation of the distance function between stable and unstable manifolds of homoclinic or heteroclinic orbits. When the Melnikov function has zero roots, it predicts the intersection of stable and unstable manifolds. Once the stable and unstable manifolds intersect transversely, they will intersect an infinite number of times. The phase space will have rapid expansion and contraction which will eventually lead to horseshoe dynamics. We only give the fundamental formulation without their calculation procedure in the following. Here we provide the details of Melnikov analysis for the system (12), expository

discussions of theory can be found in (Melnikov, 1963; Awrejcewicz & Holicke, 1999). Then we introduce following notation in system (12):

$$F(X) = \begin{pmatrix} y \\ -A\sin 2x \end{pmatrix}, G(X,t) = \begin{pmatrix} 0 \\ -\xi y + f_0 \cos \omega t \end{pmatrix}, X = \begin{pmatrix} x \\ y \end{pmatrix}, Tr(DF) = Tr \begin{pmatrix} 0 & 1 \\ -2A\cos 2x & 0 \end{pmatrix} = 0$$

we have

$$F(X_\pm(t)) \wedge G(X_\pm(t), t+\tau) = -\xi \left(y_\pm^{het}(t) \right)^2 + f_0 \cos \omega(t+\tau) y_\pm^{het}(t),$$

where $a \wedge b = a_1 b_2 - a_2 b_1$, for any $a = (a_1, a_2)^T$ and $b = (b_1, b_2)^T$, the corresponding Melnikov function of system (12) is given by

$$M(\tau, f_0, \xi, \omega) = \int_{-\infty}^{+\infty} \left[-\xi \left(y_\pm^{het}(t) \right)^2 + f_0 \cos \omega(t+\tau) y_\pm^{het}(t) \right] dt \tag{15}$$

It is clear that $y_\pm^{het}(t)$ is even function, the Melnikov function of system (12) can be re-written as

$$M(\tau, f_0, \xi, \omega) = -\xi \int_{-\infty}^{+\infty} \left(y_\pm^{het}(t) \right)^2 dt + f_0 \cos \omega\tau \int_{-\infty}^{+\infty} y_\pm^{het}(t) \cos \omega t \, dt \tag{16}$$

It can be seen that $M(\tau, f_0, \xi, \omega) = 0$ has simple zero for τ if and only if the following inequality holds:

$$\frac{f_0}{\xi} > \left| \frac{\int_{-\infty}^{+\infty} \left(y_\pm^{het}(t) \right)^2 dt}{\int_{-\infty}^{+\infty} y_\pm^{het}(t) \cos \omega t \, dt} \right| = R_{het}(\omega) \tag{17}$$

where

$$\int_{-\infty}^{+\infty} \left(y_\pm^{het}(t) \right)^2 dt = \int_{-\infty}^{+\infty} \left(\pm\sqrt{2A} \; \text{sech} \left(\sqrt{2A} \; t \right) \right)^2 dt = 2\sqrt{2A}$$

$$\int_{-\infty}^{+\infty} y_\pm^{het}(t) \cos \omega t \, dt = \int_{-\infty}^{+\infty} \left(\pm\sqrt{2A} \; \text{sech} \left(\sqrt{2A} \; t \right) \right) \cos \omega t \, dt = \pm\pi \; \text{sech} \left(\frac{\pi\omega}{2\sqrt{2A}} \right)$$

4.3 Numerical Simulation

The Melnikovian detected chaotic boundary of the approximate system is plotted by letting $f_0 / \xi = R_{het}(\omega)$ for $\lambda = 0.01,\ 0.02,\ 0.03,\ 0.04,\ 0.1,$ marked by the solid line, dashed line, dotted line, dot-dash line and thin solid line respectively, the detail seen in Figure 6(a). It is worth pointing out that there is no chaotic solution for $f_0 / \xi < R_{het}(\omega)$, conversely chaotic solution may exist in the parameter region for $f_0 / \xi > R_{het}(\omega)$, (Melnikov, 1963; Guckenheimer et al., 2007).
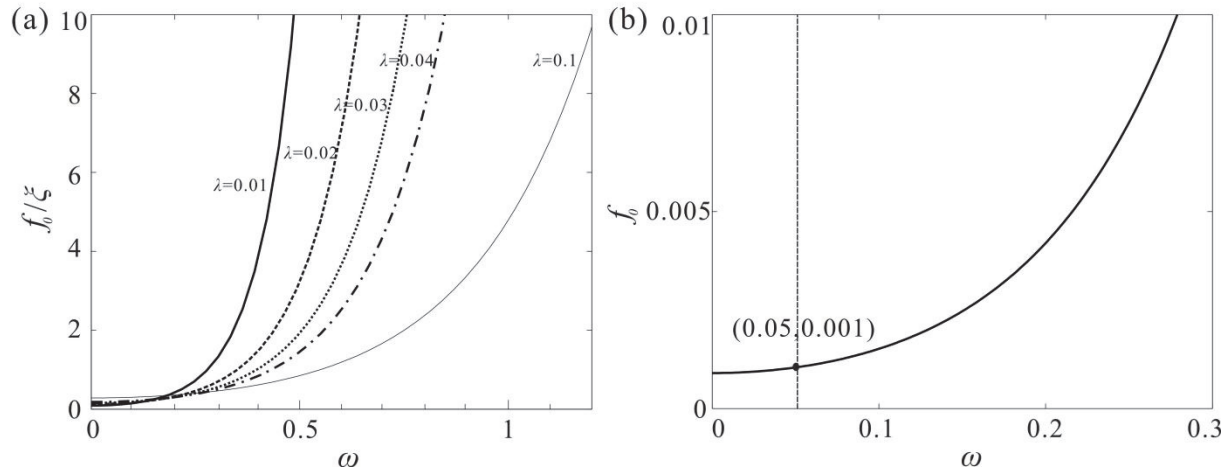
Figure 6. Graphs of the chaotic thresholds of the double heteroclinic orbits: (a) $f_0 / \xi = R_{het}(\omega)$, (b) $f_0 = \xi R_{het}(\omega)$, $\lambda = 0.01$ and $\xi = 0.01$

The Melnikovian detected chaotic boundary for the approximate system is plotted by letting $f_0 = \xi R_{het}(\omega)$ for $\xi = 0.01$, $\lambda = 0.01$ in Figure 6(b). Numerical simulations are carried out to verify the efficiency of the criteria in the following. Figure 7(a) and (b) show the comparison of bifurcation diagram between the original system (11) and its approximation (12) for f_0 versus x for parameter $\omega_0 = 1$, $\lambda = 0.01$, $\xi = 0.01$, $\omega = 0.2$ taken fixed. As can be seen in this bifurcation diagram, no chaotic motion is observed below the chaotic boundary $f_0 = 0.001$ predicted by Melnikov method which is marked by the dashed line. When f_0 increases beyond above threshold value 0.001 reaching 0.01, the system jump to the chaotic motion.
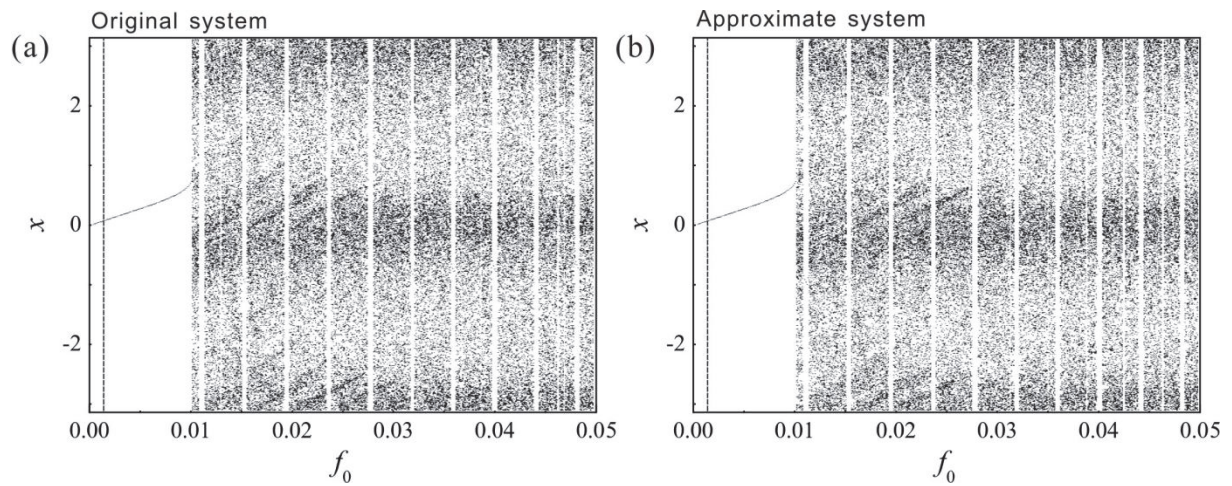

Figure 7. (a) and (b) Comparison of bifurcation diagrams between the original system (11) and approximate system (12). (Bifurcation diagrams for f_0 versus x with the chaotic threshold $f_0 = 0.001$, marked by dash line, at $\xi = 0.01, \omega = 0.05$)
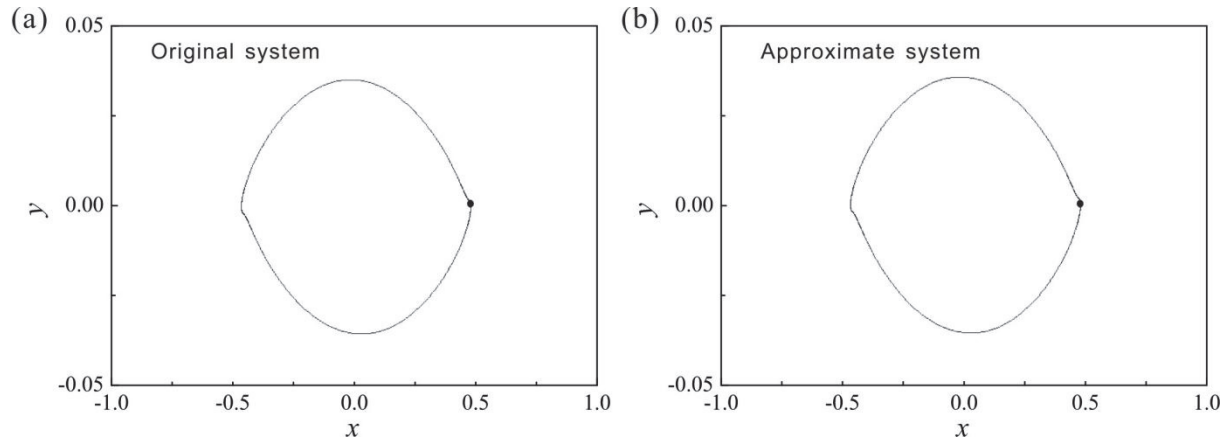
Figure 8. (a) and (b) The periodic-1 solutions of original system (11) and approximate system (12) for $f_0 = 0.008$ with their attractors marked by solid points
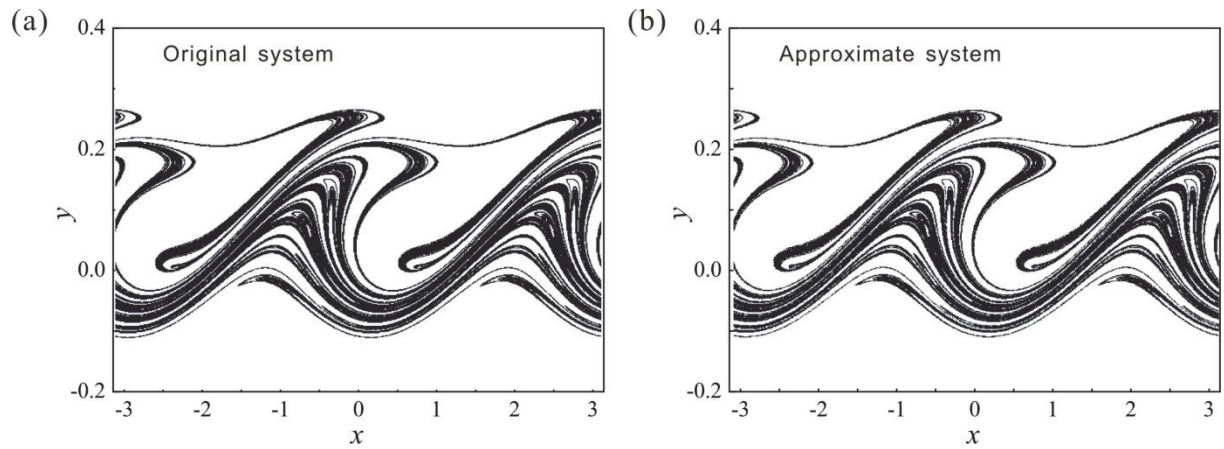

Figure 9. (a) and (b) The chaotic attractors of the original system (11) and approximate system (12) for $\xi = 0.01, \omega = 0.05, f_0 = 0.01$ with their Lyapunov characteristics $(\lambda_1, \lambda_2) = (0.024489, -0.033541), D_L = 1.73013$ and $(\lambda_1, \lambda_2) = (0.024454, -0.033544), D_L = 1.72902$, respectively
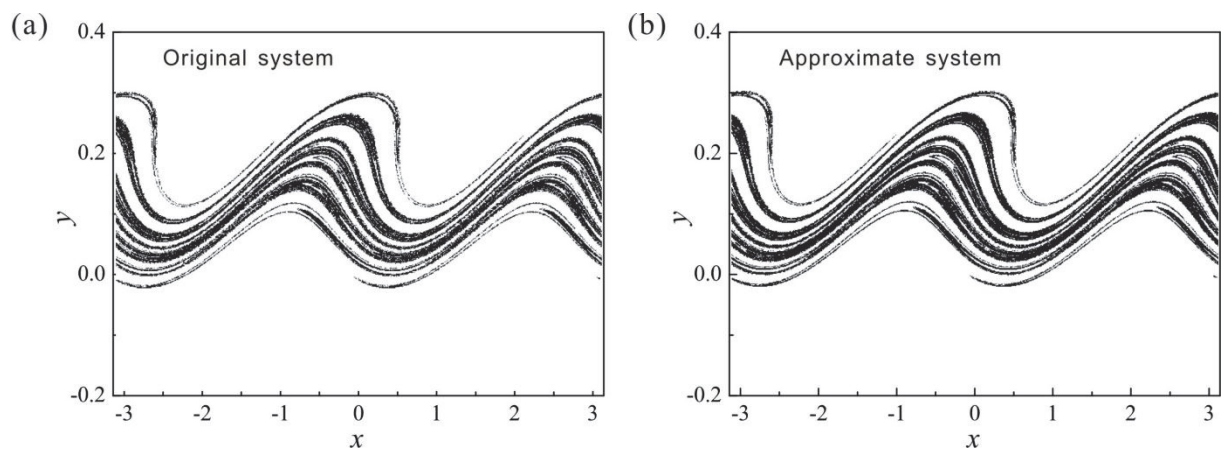

Figure 10. (a) and (b) The chaotic attractors of the original system (11) and approximate system (12) for $\xi = 0.01, \omega = 0.05, f_0 = 0.03$ with their Lyapunov characteristics $(\lambda_1, \lambda_2) = (0.023698, -0.033698), D_L = 1.70324$ and $(\lambda_1, \lambda_2) = (0.023718, -0.033717), D_L = 1.70345$, respectively

Then the comparisons between the original system (11) and its approximation (12) with the periodic-1 solutions and the attractors are shown by using numerical simulations. Comparison of the periodic-1 solutions between the

original and the approximate system are plotted in Figure 8(a) and Figure 8(b) for $f_0 = 0.008$ with their attractors marked by solid points. Chaotic attractors are calculated for the original system, shown in Figure 9(a), and the approximate system, seen in Figure 9(b), for the same parameters $\omega_0 = 1, \lambda = 0.01, f_0 = 0.01, \xi = 0.01, \omega = 0.05$. Similarly, when the parameters $\omega_0 = 1, \lambda = 0.01, f_0 = 0.03, \xi = 0.01, \omega = 0.05$, the chaotic attractors are calculated for the original system, shown in Figure 10(a), and the approximate system, seen in Figure 10(b), respectively. As can be seen in Figure 7, Figure 8, Figure 9 and Figure 10, a good degree of correlation are demonstrated in bifurcation diagram, phase portraits of periodic solution, attractor' structures and the Lyapunov characteristics, the details seen in the corresponding captions.

5. Discussion

The rotating mechanical model is developed, which is a typically cylindrical system with irrational nonlinearity. It is found that the proposed system exhibits both smooth and discontinuous dynamics due to the geometrical configuration. The unperturbed dynamics of this system with irrational terms is directly analyzed without using Taylor expansion based upon nonlinear dynamical technique, including the irrational restoring force, stability of equilibria, Hamiltonian function and phase portraits and so on. Particularly, a pair of standard double heteroclinic orbits connecting two saddle points and a pair of non-standard double heteroclinic orbits connecting two saddle-like points are proposed in both smooth and discontinuous case. The approximated chaotic boundaries of the double heteroclinic orbits have been obtained by constructing an cylindrical approximate system successfully avoiding the barrier of the associated irrational nonlinearity which completely reflects the nature dynamics of the original system for parameter taking small value. The efficiency of the proposed method have been presented by using numerical simulations, which clearly demonstrates the predicated periodic solutions and chaotic attractors. The future study on the complicated nonlinear dynamics of this cylindrical pendulum is being carried out by the current authors in two aspects: the first is the chaotic behaviors of discontinuous regime (Cao et al., 2008) and the second is the global bifurcations (Han M.A., 1999).

References

Awrejcewicz, J., & Holicke, M. M. (1999). Melnikov's method and stick-slip chaotic oscillators in very weakly forced mechanical systems, *Int. J. Bifurcat. Chaos*, *9*(3), 505-518. https://doi.org/10.1142/S0218127499000341

Cao, Q. J., Han, N., & Tian, R. L. (2011). A rotating pendulum linked by an oblique spring. *Chin. Phys. Lett.*, *28*(6), 0605021-0605024. http://dx.doi.org/10.1088/0256-/28/6/060502

Cao, Q. J., Wiercigroch, M., Pavlovskaia, E. E., & Thompson, J. M. T. (2008). The limit case response of the archetypal oscillator for smooth and discontinuous dynamics. *Int J Nonlinear Mech*, *43*, 462-73. https://doi.org/10.1016/j.ijnonlinmec.2008.01.003

Cao, Q. J., Wiercigroch, M., Pavlovskaia, E. E., Thompson, J. M. T., & Grebogi, C. (2006). Archetypal oscillator for smooth and discontinuous dynamics, *Phys. Rev. E*, *74*, 046218-046222. http://dx.doi.org/10.1103/PhysRev E.74.046218

Guckenheimer, J., & Holmes, P. (1983). *Nonlinear Oscillations, Dynamical Systems, and Bifurcations of Vector Fields*, Springer, New York.

Han, M. A. (1999). Global behavior of limit cycles in rotated vector fields. *J Differ Equ*, *151*(1), 20-35. https://doi.org/10.1006/jdeq.1998.3508

Han, N., & Cao, Q. J. (2016). Global bifurcations of a rotating pendulum with irrational nonlinearity, *Commun. Nonlinear Sci. Numer. Simulat.*, *36*, 431-445. http://dx.doi.org/10.1016/j.cnsns.2015.12.009

Han, N., & Cao, Q. J. (2017). A parametrically excited pendulum with irrational nonlinearity. *Int J Nonlinear Mech*, *88*, 122-134. http://dx.doi.org/10.1016/j.ijnonlinmec.2016.10.018

Han, N., Cao, Q. J., & Liang, T. W. (2015). A rotating disk linked by a pair of springs, *Nonlinear Dyn.*, *78*, 1275-1291. http://dx.doi.org/10.1007/s11071-014-1742-1

Han, N., Cao, Q. J., & Wiercigroch, M. (2012). Estimation of the chaotic thresholds for the recently proposed rotating penulum, *Int. J. Bifurcation Chaos, 23*, 13500741-22.

http://dx.doi.org/10.1142/S0218127413500740

Koch, B. P., & Leven R. W. (1984). Subharmonic and Homoclinic Bifurcations in a Parametrically Forced Pendulum. *Physica D*, *16*, 1-13. http://dx.doi.org/10.1016/ 0167-2789(85)90082-X

Kwek, K. H., & Li, J. B. (1996). Chaotic Dynamics and Subharmonic Bifurcations in a Nonlinear System. *Int. J. Non-linear Mech.*, *31*(3), 277-295. https://doi.org/10.1016/0020-7462(95)00068-2

Melnikov, V. K. (1963). On the stability of the center for time periodic perturbations, *Trans. Moscow. Math.*, *12*, 1-57.

Tian, R. L., Cao, Q. J., & Yang, S. P. (2010). The codimention-two bifurcation for the recent proposed SD oscillator. *Nonlinear Dyn., 59,* 19-27. https://doi.org/10.1007/s11071-009-9517-9

Wiggins, S. (1988). *Global Bifurcations and Chaos, Analytical Methods*, Springer, New York.

Xu, X., & Wiercigroch, M. (2007). Approximate Analytical Solutions for Oscillatory and Rotational Motion of a Parametric Pendulum. *Nonlinear Dyn.*, *47,* 311-420. http://dx.doi.org/10.1007/s11071-006-9074-4

Yabuno, H., Miura, M., & Aoshima, N. (2004). Bifurcation in anInverted Pendulum with Tilted High-Frequency Excitation: Analytical and Experimental Investigations on the Symmetry Breaking of the Bifurcation. *J. Sound Vib.*, *273*, 493-513. https://doi.org/10.1016/S0022-460X(03)00507-8